Atmospheric Research 291 (2023) 106819

Contents lists available at ScienceDirect

Atmospheric Research

journal homepage: www.elsevier.com/locate/atmosres

A new method to estimate aerosol radiative forcing on photosynthetically active radiation

Inmaculada Foyo-Moreno [a,b,*], Ismael L. Lozano [c,d], Inmaculada Alados [a,e], Juan Luis Guerrero-Rascado [a,b]

[a] Andalusian Institute for Earth System Research, Granada 18006, Spain
[b] Department of Applied Physics, University of Granada, Granada 18071, Spain
[c] Department of Forest Sciences, University of Helsinki, Helsinki 00014, Finland
[d] Institute for Atmospheric and Earth System Research, University of Helsinki, Helsinki 00014, Finland
[e] Applied Physics II Department, University of Málaga, Málaga 29071, Spain

ARTICLE INFO

Keywords:
Aerosols
Photosynthetically active radiation
Radiative forcing

ABSTRACT

A new method to estimate aerosol radiative forcing (ARF) on photosynthetically active radiation (PAR) is proposed using as input only the solar position and global irradiance measurements, available in many radiometric stations worldwide. The main contribution of this work is the proposal of a new and simple tool (max-k_t method) based in the parameterization of the envelope of the relationship between clearness index (k_t) and the solar position. To this aim, a 1-year database (2020) of cloud-free data acquired in a Southwest Mediterranean site was used for the proposal and two more years (2017 and 2018) were used to extend the results. The ARF values retrieved using the new method were compared with estimates calculated by two physical models widely employed in the literature, such as the SBDART (Santa Barbara DISORT Atmospheric Radiative Transfer model) and an improved version of the CPCR2 (Code for Physical Computation of Radiation, 2 bands) model. The new method provided ARF values of the order of those provided by these physical models, especially with the SBDART model, confirming the validity of this new method. An ARF seasonal pattern was found with higher values in summer, $(-30{,}7 \pm 9{,}0)$ Wm^{-2} in August during 2017, $(-40{,}1 \pm 11{,}8)$ Wm^{-2} in June during 2018 and $(-28{,}8 \pm 7{,}7)$ Wm^{-2} in July during 2020 and minimum values in winter, $(-8{,}1 \pm 5{,}1)$ Wm^{-2} in January during 2017, $(-5{,}7 \pm 5{,}8)$ Wm^{-2} in December during 2018 and $(-7{,}8 \pm 5{,}4)$ Wm^{-2} in December during 2020. Moreover, a dependence on solar zenith angle (θ_z) was detected excepting during the year 2018, increasing ARF absolute values at θ_z from 0° to 45°-60° and decreasing to zero for the Sun near the horizon. This technique is very useful due to the difficulty of knowing all the inputs requested by the physical models.

1. Introduction

Solar radiation is the primary energy source for life on Earth (Wild, 2009), and the portion of global solar radiation covering the visible spectral range (400–700 nm), i.e. the photosynthetically active radiation (PAR), plays a fundamental role for the vegetation, since PAR directly drives the photosynthesis process. Thus, the knowledge of PAR is a prerequisite for modelling the terrestrial ecosystem productivity (Jacovides et al., 2007), specifically for plant productivity modelling in forests (Landsberg and Waring, 1997), for biomass production and for natural illumination in greenhouses (Alados et al., 1996; Ramírez-Pérez et al., 2017). Moreover, PAR is crucial to aquatic primary production, and the knowledge of PAR is necessary to estimate the euphotic depth of the oceans (Luthala et al., 2013). Accurate PAR measurements have a main role to determine deforestation and climate change impacts on agriculture (Pei et al., 2013; Zempila et al., 2016). Besides, PAR is a key factor controlling ecological processes such as the terrestrial carbon and hydrological cycles (Potter et al., 2007, 2008; Jonard et al., 2020). However, despite its importance, a global routine network for measuring PAR has not yet been established. This lack of measurements leads to the use of different alternatives in order to estimate PAR. There are different estimation methods in the literature, which can be classified into three categories, namely physically-, empirically- and satellite-based models. Other authors to estimate global irradiance at different ranges of

* Corresponding author at: Andalusian Institute for Earth System Research, Granada 18006, Spain.
E-mail address: ifoyo@ugr.es (I. Foyo-Moreno).

https://doi.org/10.1016/j.atmosres.2023.106819
Received 16 January 2023; Received in revised form 12 May 2023; Accepted 17 May 2023
Available online 20 May 2023

wavelengths on surface have developed a hybrid method combining deep neural network and a radiative transfer model using Himawari-8 satellite data (Ma et al., 2020).

The two main factors affecting solar irradiance are clouds and atmospheric aerosols, being aerosols the most important under clear skies. Atmospheric aerosols are known to affect the atmospheric transmittance through the scattering and absorption of sunlight (direct effect), and modifying clouds properties (indirect effect), such as the cloud albedo effect (enhancement of cloud albedo due to smaller droplets) (Twomey, 1974) or the cloud lifetime effect (extension of cloud lifetime due to smaller droplets and less precipitation) (Albrecht, 1989). These indirect effects can have an even larger impact than the direct effect at the top of the atmosphere (Lohmann and Feichter, 2005). Consequently, atmospheric aerosols alter the Earth's surface budget with strong impacts on the interactions between the atmosphere and biosphere, not only by altering the radiation balance but also by mediating feedbacks between vegetation and climate (Mercado et al., 2009; Mahowald et al., 2011; Stocker et al., 2013). Consequently, it is crucial the knowledge of aerosol radiative effects, however, aerosol radiative effects and its relationship to climate change remain inaccurate (Stocker et al., 2013), being this uncertainty large in the PAR range because of the scarcity of related studies (Lyamani et al., 2006a; Mateos et al., 2014; Zhu et al., 2015).

To evaluate aerosol radiative effects, the concept of aerosol radiative forcing (ARF) is introduced. ARF is defined as the change in the net radiation (difference between the downward and the upward irradiances at the Earth's surface) due to variations in the atmospheric aerosol properties with respect to an aerosol-free atmosphere. Therefore, it is necessary to select clear skies to avoid the cloud effects.

When there are no available cloud measurements, different methods can be used to identify clear sky conditions from ground irradiance measurements. Younes and Muneer (2007) presented an overview of several clear sky detection algorithms, all of them using indexes derived from global and diffuse irradiances, with their evaluation. The simplest criterion uses the clearness index (k_t), defined as the ratio between the global irradiance and the extraterrestrial global irradiance, both on a horizontal surface. This index takes into account the aerosols and clouds effects in atmospheric transparency. Also, the diffuse to global solar radiation ratio (k) can be used to identify clear skies. High k_t and low k values are both representative of clear skies. In this sense, previous studies have used different thresholds for k_t to identify clear skies. For example, Iqbal considers a clear-sky to be represented by k_t between 0,7 and 0,9, and Lanetz et al. (2005) did not restrict an upper limit of k_t for clear-sky arguing the fact that this limit is not static, depending on the site. On the other hand, a k value lower than 0,3 is usually proposed (e.g. Lefèvre et al., 2013). Thevenard and Brunger (2001) used a k value between 0,2 and 0,4, and other authors have proposed more complex indexes including dependencies on the solar zenith angle (θ_z) (e.g., Perez et al., 1990; Alados et al., 2000). For these procedures, the method proposed by Long and Ackerman (2000) is considered as a standard for data quality control in the solar measurement community. Their approach comprises four tests that use global and diffuse irradiance measurements.

There are different methods to estimate ARF. One is the so-called direct method (Satheesh and Ramanathan, 2000) that previously requires the aerosol forcing efficiency (AFE), defined as the irradiance variation per unit of aerosol optical depth (AOD) to estimate ARF (Charlson et al., 1991). In this method, AFE is calculated through the linear fit of net irradiance versus aerosol optical depth (AOD) for a given solar zenith angle (θ_z). Its advantage lies in the fact that the AFE is directly estimated from observations, without further assumptions about the radiative fluxes under aerosol-free conditions. Finally, ARF in this method is derived by multiplying AFE and AOD. This method has been previously used by several authors (e.g. Antón et al., 2011; Foyo-Moreno et al., 2014; Lozano et al., 2021). The other method mostly used by researchers (the so-called indirect method) is to simulate solar irradiance values through radiative transfer models such as the SBDART model (Santa Barbara DISORT Atmospheric Radiative Transfer model; Ricchiazzi et al., 1998) using aerosol properties obtained from AERONET measurements (Aerosol Robotic Network; Holben et al., 1998) as input and simulations under aerosol-free conditions are also required.

Existing radiative transfer models propose different approaches to solve the radiative transfer equation. What differentiates one model from another is the structure of the atmosphere, the number of input parameters and model complexity. Model-model comparisons have shown that different radiative transfer codes may agree well if they are run with identical optical properties as input (Halthore et al., 2005). The SBDART model is selected here by its high accuracy (Li et al., 2010), besides it has been consistently developed over the past few decades (Kundu et al., 2018) and has been extensively applied to ARF in studies of atmosphere energy budget and also in satellite remote sensing (Luo et al., 2019).

In this work a new method to estimate ARF is proposed, requiring only global irradiance measurements (which are available in many radiometric stations), with the added value of aerosol measurements not needed. The main contribution of this work is the proposal of a new and simple tool (max-k_t method) to estimate for PAR considering only the dependence of the clearness index with solar position through the cosine of θ_z, that is, only measurements of global radiation are needed. From the maximum envelope of the dependence of k_t with the cosine of θ_z, an equation of general validity is obtained but with coefficients that are dependent on the site. Here, the measurements acquired at an urban middle-latitude site in the Mediterranean basin during one year (2020) have been used to propose the new method. The results are compared with estimations obtained from the indirect methods using the modified CPCR2 parametric model (Code for Physical Computation of Radiation, 2 bands) and the SBDART model (Alados-Arboledas et al., 2000) and two more years (2017 and 2018) have been used to extend the results.

2. Experimental site and dataset

The measurements used in this study were collected at the radiometric station installed on the roof of the IISTA-CEAMA building at Granada (37,164 ^{o}N; 3605 ^{o}W; 680 m.a.s.l.), an urban site located in the Southeast of Spain in the West Mediterranean region. This radiometric station is managed by the Atmospheric Physic Research Group (GFAT) at the University of Granada and is part of the observatory AGORA (Andalusian Global ObservatoRy of the Atmosphere) in the framework of ACTRIS (Aerosol, Clouds and Trace Gases Research Infrastructure). Granada presents large seasonal temperature differences, characterized by cool winters and hot summers, with a mean temperature for the year 2020 of (21,6 $\pm$ 8,2) ^{o}C, with the extreme values between -1,9 and 40,5 °C. Main local aerosols sources are traffic, local mineral dust during the dry season, anthropogenic aerosols in winter from fuel oil combustion for domestic heating and also biomass burning in summer (agricultural waste burning) (Titos et al., 2012, 2017) and bioaerosols, especially pollen grains emitted by urban and periurban vegetation (Cariñanos et al., 2021, 2022; Ramírez-Aliaga et al., 2022). Others aerosol sources are continental aerosols from Europe and during the spring and summer season dust mineral from Sahara desert located in North Africa (Guerrero-Rascado et al., 2008, 2009; Lyamani et al., 2006a, 2006b, 2010), also transported smoke from North America, North Africa and Europe (Alados-Arboledas et al., 2011; Baars et al., 2019; Ortiz-Amezcua et al., 2014, 2017; Titos et al., 2017; Sicard et al., 2019). Extraordinarily, there are aerosols events from volcanic plumes (Navas-Guzman et al., 2013; Sicard et al., 2012), and oceanic aerosols from Arctic and Atlantic oceans or maritime aerosols from the Mediterranean Sea (Pérez-Ramírez et al., 2016).

One full year of PAR data and aerosol properties during 2020 has been used to propose this method and others two years (2017 and 2018) to extend the results. One-minute measurements of Photosynthetically Active Radiation (PAR) (400–700 nm) were measured with a SKP 215 PAR Quantum Sensor manufactured by Skye Instruments. This

instrument uses a blue enhanced planar diffused silicon detector with a sensitivity of 0,015 $\mu A \mu mol^{-1} m^{-2} s^{-1}$. The quantum sensor has a maximum relative error < 5% relative to the values measured. Simultaneous one-minute measurements of total solar irradiance were recorded with a radiometer CM11 manufactured by Kipp&Zonen. This instrument measures broadband solar irradiance (280–2800 nm) and complies with International Organization for Standardization (ISO) 9060 criteria for an ISO secondary standard pyranometer. Both measurements were recorded in a CR10X data logger manufactured by Campbell Scientific.

Additionally, Aerosol Optical Depth (AOD) values, measured every 15 min by a CIMEL Sun/sky photometer (CE-318-4) were used in this study. This equipment is part of the AErosol RObotic NETwork (AERONET; Holben et al., 1998) and it has been routinely measuring at Granada station of Andalusian Global ObseRvatory of the Atmosphere (AGORA), located on the rooftop of IISTA-CEAMA, since 2004. This instrument measures direct solar irradiance with a 1,2° full field of view at 340, 380, 440, 500, 675, 870, 940 and 1020 nm as well as sky radiances in the almucantar and principal plane geometries at 440, 675, 870 and 1020 nm. All radiance measurements are processed following the AERONET protocol as described by Holben et al. (1998), obtaining columnar aerosol properties at different quality levels (1.0, 1.5, 2.0). AOD level 2.0 version 3 data, the highest quality AERONET data (Giles et al., 2019), were used in this study. AOD data have a total uncertainty of 0,01 for wavelengths ≥440 nm and 0,02 for shorter wavelengths (Holben et al., 1998). The Sun-photometer also provides the surface albedo measurements used in this study at 440, 675, 870 and 1020 nm with a total uncertainty of 0,02 (Foyo-Moreno et al., 2014).

3. Methodology: clear-sky DATA selection

Considering the definition of ARF given in section 1, firstly it is necessary to select clear-sky data. Previously to the acquisition of clear-sky data from all-sky datasets, a deep quality control has been applied in order to detect and remove potential erroneous measurements, following Lozano et al. (2021). In this work, the data-sets include the seasonal features, solar geometries and meteorological conditions, leading to check the performance of the proposed method.

The more usual procedures to detect clear skies use k_t and k indices as described in section 1, but since diffuse irradiance measurements may not be available at many radiometric stations, here two criteria have been evaluated using only one index, i.e.: k_t, in comparison to the cases detected by visual inspection. This method consists in representing a daily scatter plot of the global irradiance against time for each day of the dataset. When the plots do not follow the symmetrical typical pattern for clear skies with the maximum value centered at solar noon, these data are attributed to cloud presence and, consequently, discarded. The first one is the simplest criterion (criterion#1), based on k_t values above a threshold of 0,7. The second one (criterion#2) includes the dependence of k_t on solar position (Alados and Alados Arboledas, 1999). The authors analyzed k_t for cloudless skies conditions (zero octas for cloudiness), evidencing the great influence on θ_z. Thus, they fitted this dependence by means of a polynomial function of cos θ_z. A threshold for the cloudless sky conditions was defined by subtracting from this equation the standard deviation associated to the independent coefficient of this polynomial function. In this sense, the criterion for cloudless sky conditions reads as follows:

$$k_t > 0,53 + 0,31 cos\theta_z - 0,15\ cos^2\theta_z \quad (1)$$

Fig. 1 shows experimental PAR values versus the solar position for the selection of clear days according to the different criteria aforementioned. The worst criterion is to consider cases with k_t above a threshold because they can also include cloudy cases. In this sense, it is also interesting to point out that values above of the clear skies correspond to enhancement values by the clouds and values below are associated to clouds with the natural cloud effects of attenuation. Both criterions using k_t are not very restrictive as observed from Fig. 1, including some cloudy cases, consequently, in this work the selection of clear skies was made through supervised inspection considering the typical pattern followed by the global irradiance along the day in order to detect misclassified data points. Although a lot of methods are available in the literature, which can identify clear sky conditions from ground measurements, it is important to detect correctly clear periods because this is the main basis of the proposal of this work.

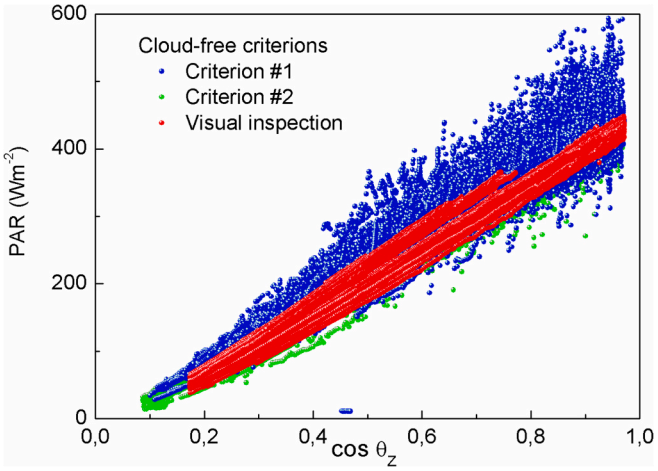

Fig. 1. Photosynthetically active radiation (PAR) versus cosine of solar zenith angle (cos θ_z) for clear skies considering different criteria.

4. Models description to estimate ARF: SBDART and modified CPCR2

In this section, two models are described to estimate ARF with the indirect method. As presented in section 1, ARF is defined as the difference between the measured net irradiance (F_{net}) and the same magnitude for an aerosol-free atmosphere ($F_{net,a}$):

$$ARF = F_{net} - F_{net,a} \quad (2)$$

where F_{net} is the difference between the downward and the upward irradiances at the Earth's surface and $F_{net,a}$ is the same but without aerosols. Net irradiances under the aerosols presence/absence can be written, respectively, as:

$$F_{net} = (1 - A)\ PAR \quad (3)$$

$$F_{net,a} = (1 - A)\ PAR_a \quad (4)$$

where PAR represents the measured PAR values, PAR_a is the estimated irradiance under absence of aerosols, and A is the surface albedo. Thus, ARF is:

$$ARF = (1 - A)\ (PAR - PAR_a) \quad (5)$$

In this work, the surface albedo was set to 0,14 corresponding to the annual average value at 675 nm provided by AERONET at our study area, taking into account the results obtained in the previous work of Lozano et al. (2021) considering a 11-year dataset at the same experimental site. The overall error in net flux increases by <0,3% due to the uncertainty in surface albedo (Di Biagio et al., 2010).

4.1. SBDART model

To simulate PAR values for clear-sky, the SBDART model (Ricchiazzi et al., 1998) has been adopted for many researchers in previous studies (e.g. Huang et al., 2020; Khan et al., 2012; Xia et al., 2007a, 2007b). This

model resolves the plane-parallel radiative transfer equation in clear and cloudy conditions within the atmosphere and at the Earth's surface (Ricchiazzi et al., 1998), and is applied in studies of atmosphere energy budget and satellite remote sensing (e.g. Luo et al., 2019; Liang et al., 2019). The model is based on the DISORT (Discrete Ordinates Radiative Transfer Program for a Multi-Layered Plane-Parallel Medium), the low-resolution band model developed for LOWTRAN 7 atmospheric transmission, and the Mie scattering results for light scattering by water droplets and ice crystals (Ricchiazzi et al., 1998), and have been consistently developed over the past few decades (Kundu et al., 2018). The model includes six different standard atmospheric profiles, four standard aerosol types along with its vertical distribution and five surface types. SBDART considers all the processes that affect both absorption and scattering processes at the ultraviolet, infrared and visible spectral ranges.

The radiative transfer model was run using as inputs the middle-latitude standard atmosphere for winter and summertime and aerosols in the urban boundary layer. The cosine of solar zenith angle, surface albedo, aerosol optical depth, surface atmospheric pressure and surface relative humidity has been also employed as experimental measurements inputs for the computations. A fixed AOD_{500} value of 0,05 was used as background aerosol corresponding with the percentile 10th value of the study period for the radiative solar irradiance calculations. AOD_{500} has been used instead of AOD_{550} for the radiative transfer model input, due to the fact of the absence of AOD_{550} measurements, besides a strong correlation is found between AOD_{500} and the ARF (Prasad et al., 2007).

4.2. Modified CPRC2 model

CPCR2 is a two-band model proposed for clear-sky Gueymard (1989). The solar spectrum is divided into an ultraviolet/visible band (290–700 nm) and an infrared band (700–2700 nm). In our case, considering the wavelength covered by the photosynthetically active spectrum only the first band is relevant. This model computes broadband transmittances for the different atmospheric extinction processes. The use of these transmittances allows for the computation of the direct beam component. For the diffuse component some approximations have been used in order to parameterize the complexity of the scattering process. The diffuse component is modelled as a combination of three individual contributions: molecules, aerosols and the backscattering process between ground and sky. The diffuse irradiance due to multiple reflections between the Earth's surface and the atmosphere depends on the ground albedo, and on the sky albedo, both values have been considered wavelength independent and the expression for sky albedo proposed by Justus and Paris (1985) is used, according to the diffusion approximation (Kondratyev, 1969). More details also can be found in Olmo et al. (2001). Finally, the global irradiance is obtained by combination of the direct irradiance projected onto the horizontal surface and the diffuse horizontal irradiance.

The modified CPCR2 model is an improved version developed by Gueymard (1989) made in the work of Alados-Arboledas et al. (2000). The modifications provide a better estimate of the direct and global components of PAR. This improvement is achieved by introducing some modifications concerning the parameterization of the aerosol and molecular contribution to the diffuse component. There are two modifications in this parameterization. The first modification builds on a previous one proposal by Bird and Riordan (1986) used in the spectral code SPECTRAL-2. The second consists in modifying the contribution of aerosols, including the simple scattering albedo (ω_o) as a multiplying factor, following a procedure similar to that included in parameterization Model A Iqbal (Iqbal, 1983). The best results are obtained using a ω_o value of 0,750. The estimation of the direct component improves the use of an exponent α, which is a function of relative humidity as proposed by Gueymard. More details can be found in Alados-Arboledas et al. (2000) and Alados et al. (2002).

5. Results and discussion

5.1. Clearness index for clear skies

Fig. 2 shows the measured PAR versus solar position (through the cosine θ_z) for different ranges of k_t in 0,1-steps. This index varied between 0,41 and 0,83, with a mean value of 0,72 ± 0,06 for clear-skies and a mean value of 0,59 ± 0,22, a mode value of 0,73, a median value of 0,68 and an interquartile range (the difference between the third and the first quartile) of 0,29 for all-skies. A clear dependence of PAR on k_t is observed, increasing with k_t. Now, Fig. 3 shows the relationship between k_t and cos θ_z but only for all selected clear skies obtained as described in Section 3.1.

Fig. 3 evidences a nonlinear dependence in the relationship between k_t and cos θ_z, finding a high spread in the cloud points, especially for the central values of k_t, for a fixed solar position, when the Sun is close to the horizon. Therefore, this dependence of k_t on cos θ_z invalidates the k_t-based criterion to identify clear skies, in addition to this limit is site-dependent as suggested by Lanetz et al. (2005). The positive dependence of k_t on solar position indicates higher values of k_t when the Sun is close to zenith. Moreover, it is possible to parameterize two enveloping curves for the maximum and minimum possible values of k_t at a given solar position (Fig. 3), given by second order polynomial equations:

$$k_{t,min,max} = A + B\ cos\ \theta_z + C\ cos^2\theta_z \quad (6)$$

where A, B, and C are the fitting coefficients (A = 0,56; B = 0,62; C = −0,36). These two enveloping curves correspond to extreme sky conditions, with $k_{t,min}$ representing less transparency, due to a major aerosol load and, conversely, $k_{t,max}$ representing large transparency, affected only by the aerosol background. This fact constitutes the basis of the new method proposed in the next section.

5.2. New proposed method

Following the previous section, it is possible to parametrize $k_{t,max}$ under clear skies for a given solar position, corresponding to the aerosol background of the site. Thus, using the model to estimate PAR for all sky conditions (Foyo-Moreno et al., 2017), that is PAR = 586 k_t cos θ_z in units of Wm^{-2}, it is possible to replace in that model k_t by $k_{t,max}$ with eq. 5 and, thus, to obtain PAR under clear skies with background aerosols (PAR_a) as:

$$PAR_a = 586\ k_{t,max}\ cos\theta_z \quad (7)$$

Thus, inserting eq. 6 into eq. 5, the new method proposed to estimate

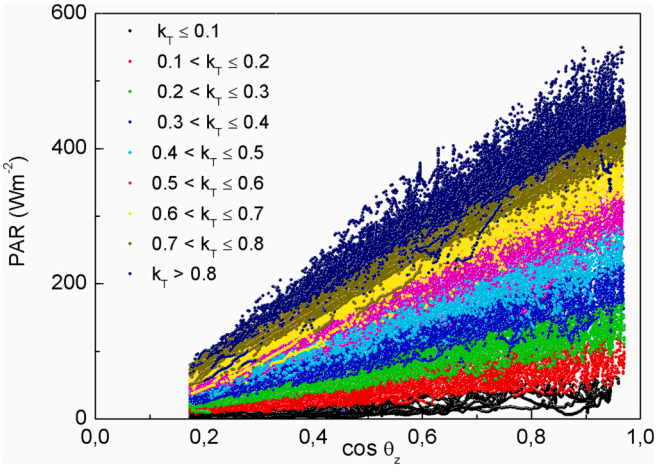

Fig. 2. Photosynthetically active radiation (PAR) versus cosine of solar zenith angle (cos θ_z). Different clearness index (k_t) values are represented by different colors.

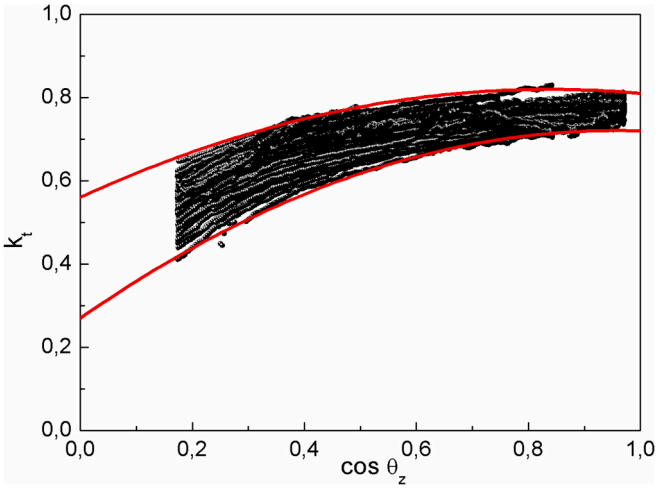

Fig. 3. Clearness index (k_t) with the cosine of solar zenith angle (cos θ_z) for clear skies. Dots represent experimental data. Red line represents the enveloping curve. (For interpretation of the references to colour in this figure legend, the reader is referred to the web version of this article.)

ARF is:

$$ARF = (1-A)\,586\,cos\,\theta_z\left(k_t - k_{t,max}\right)$$
$$= (1-A)\,586\,cos\,\theta_z\left(k_t - 0,56 - 0,62\,cos\,\theta_z + 0,36\,cos^2\theta_z\right) \quad (8)$$

From now, this new method is known as the max-k_t method.

Fig. 4 shows the ARF seasonal evolution with the proposed max-k_t method (eq. 8) showing the monthly mean values along with the standard deviation. A clear seasonal pattern is seen, with the aerosol radiative effects stronger during summer months, (−30,7 ± 9,0) Wm^{-2} in August during 2017, (−40,1 ± 11,8) Wm^{-2} in June during 2018 and (−28,8 ± 7,7) Wm^{-2} in July during 2020 and minimum values in winter, (−8,1 ± 5,1) Wm^{-2} in January during 2017, (−5,7 ± 5,8) Wm^{-2} in December during 2018 and (−7,8 ± 5,4) Wm^{-2} in December during 2020. These results are in accordance with previous results obtained for the same location (Granada). Thus, Lozano et al. (2021) for a long period (2008–2018) found values between −30 Wm^{-2} and -14 Wm^{-2} at 15° and − 9 Wm^{-2} and + 3 Wm^{-2} at 75°. Other authors, using the SBDART model to estimate the solar irradiance without aerosols, also found this seasonal pattern with maximum values for ARF in summer and minimum values in winter for a Mediterranean urban coastal site, (Valencia, Spain) for the period 2003–2011, in the spectral range (305–2800 nm) (e.g. Esteve et al., 2014). This annual variability observed in the Mediterranean by different authors is associated with the variability of AOD (e.g. Bergamo et al., 2008). Lozano et al. (2021) for a 11-year period in Granada found the largest monthly mean AOD_{500} in summer (0.16 at July and August) meanwhile the lowest values are in winter (0.08 at November and December). For the data used in this work, the maximum values have been obtained in August during the year 2017 and 2018 (0,19 and 0,22, respectively) and in July (0,21) during 2020 and the minimum have been obtained in December for all years (0,06 for 2017 and 0,07 for 2018 and 2019), although in 2017 was a higher maximum in February due to an unprecedented extreme Saharan dust event registered from 20 to 23 February 2017 over the Iberian Peninsula (Fernández et al., 2019). The maximum (minimum) values occur in summertime (wintertime) due to the higher (lower) frequency Saharan dust outbreaks over the Mediterranean region (Salvador et al., 2014; Gkikas et al., 2013, 2018).

A higher scatter is also observed in Fig. 4 during central months of the year. This can be related also to the higher likelihood of desert dust and biomass burning events over the Iberian Peninsula in summer (e.g., Cachorro et al., 2008; Valenzuela et al., 2012). The higher occurrence of large aerosol loads during the warm seasons explains the more negative ARF during summer, because the influence of mineral dust aerosol (with high AOD) causes strong radiative effects, as was also reported by previous studies (e.g. Guerrero-Rascado et al., 2009; Antón et al., 2011; Román et al., 2013; Garcia-Herrera et al., 2014). Precisely, in summer the frequency of dust intrusions at Granada is very high (52%) as reported by Foyo-Moreno et al. (2019) for the period 2010–2012. In fact, for the year 2020, the mean value lowest found for the Angström parameter has been at August (0,73 ± 0,45) and also for this month has been obtained the lowest mean value for the fine mode fraction (FMF) with a value of (0,43 ± 0,18). Foyo-Moreno et al. (2019) proposed a classification scheme based on FMF for distinguishing the different aerosol types. This method is based on the previous work of Lee et al. (2010) that uses two parameters to classify aerosol types, namely FMF and single scattering albedo (ω_o). Following the criterion by Foyo-Moreno et al. (2019), in this work it has been found 65% of cases of Saharan dust intrusions in summer season for the year 2020.

In order to take into account the solar position effect on ARF, an additional analysis was performed considering up to six categories in θ_z: 1 ($\theta_z \leq 15°$), 2 ($15° < \theta_z \leq 30°$), 3 ($30° < \theta_z \leq 45°$), 4 ($45° < \theta_z \leq 60°$), 5 ($60° < \theta_z \leq 75°$), 6 ($\theta_z > 75°$) (Fig. 5). A dependence of ARF on solar zenith angle was found for the three years, with a clear pattern increasing ARF (in absolute values) as increasing θ_z and an inflection point (not detected for the year 2018) at the 45°-60° range, with the maximum value of (−32,4 ± 8,9) Wm^{-2} for the year 2018 and of (−30,2 ± 8,5) Wm^{-2} for the year 2020. This result was also found by Lozano et al. (2021) using the direct method for a long dataset at Granada. This trend is similar to that obtained by Meloni et al. (2005) but the trend is reversed for highly absorbing aerosols. Also, Di Biagio et al. (2009) pointed out that this trend depends on the aerosol type and seems to be reversed for urban/industrial-biomass burning aerosols. Additionally, several authors suggested that the inflection point in this trend depends on the aerosol properties (Di Biagio et al., 2010).

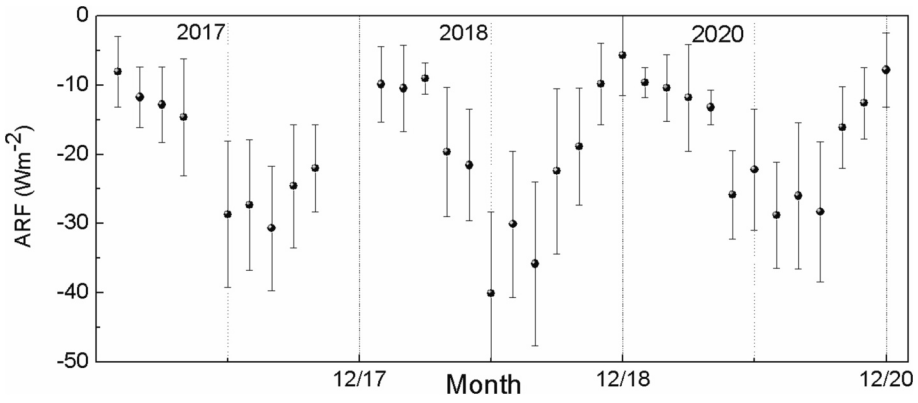

Fig. 4. Aerosol radiative forcing (ARF) mean values along with its standard deviation by month.

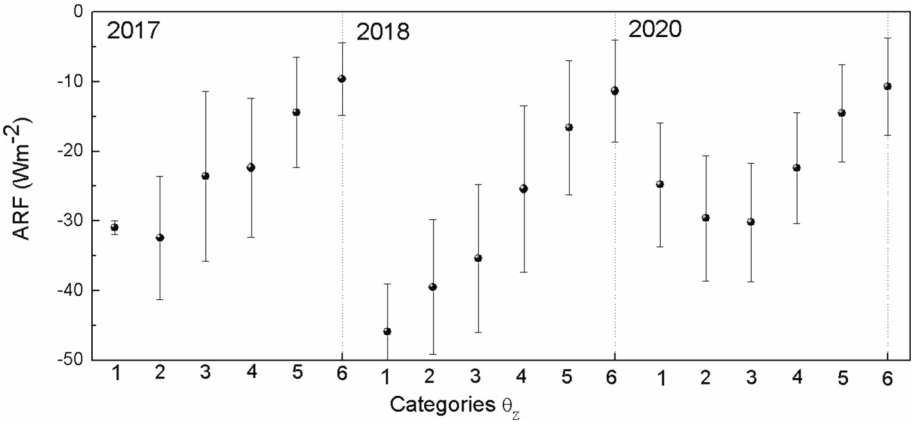

Fig. 5. Aerosol radiative forcing (ARF) mean value with its standard deviation level by solar zenith angle categories.

5.3. Comparison with other models

In general, higher ARF values by the new method have been retrieved with a mean value of (−20 ± 11) Wm^{-2} varying between −63 and + 18 Wm^{-2} during the year 2017, a mean value of (−27 ± 14) Wm^{-2} varying between −69 and + 11 Wm^{-2} during the year 2018 and a mean value of (−23 ± 11) Wm^{-2} varying between −53 and + 1 Wm^{-2} during the year 2020. The values obtained by the SBDART model varied between −50 and + 46 Wm^{-2} with a mean value of (−2 ± 8) Wm^{-2} during the year 2018, between −21 and − 3 Wm^{-2} with a mean value of (−12 ± 5) Wm^{-2} during the year 2018 and between −19 and − 2 Wm^{-2} with a mean value of (−14 ± 4) Wm^{-2} during the 2020. However, the CPCR2 model presents a very low amplitude with a mean value of (−42 ± 2) Wm^{-2} varying between −47 and − 36 Wm^{-2} during the year 2017, with a mean value of (−36 ± 2) Wm^{-2} varying between −40 and − 31 Wm^{-2} for the year 2018 and similar values for the year 2020.

Considering the definition of ARF (which includes the terms PAR under clear skies with and without aerosols, PAR and PAR_a, respectively), the differences between the three estimations come from the calculations of PAR and PAR_a. Thus, Fig. 6 for the year 2020 shows the estimated PAR values for clear skies without aerosol versus cos θ_z, and Fig. 7 shows the estimated PAR values versus experimental values for real situations, i.e., with aerosol. The main differences between the three models came from the estimations of PAR with aerosol background values (Fig. 6) since the simulations under clear skies with aerosol are very close. Anyway, from Fig. 7, comparing the estimations of PAR with experimental values, it can be concluded that the model presented in Foyo-Moreno et al. (2017) shows a better performance, close to the line 1:1 and with a slope of 0,9997 ± 0,0002.

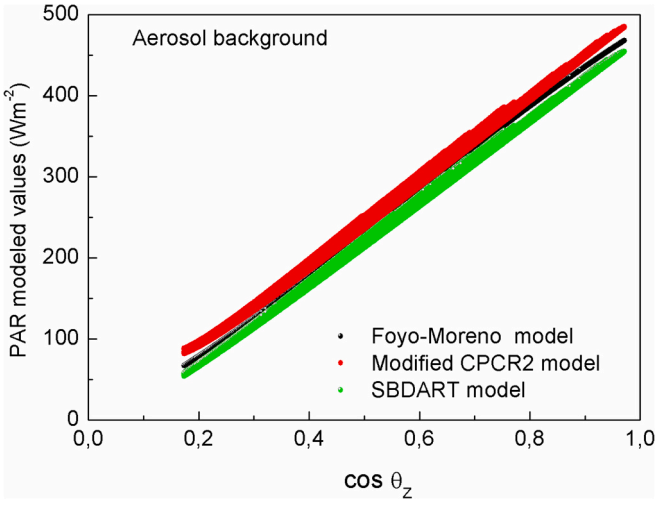

Fig. 6. Comparison of Photosynthetically active radiation (PAR) modelled values obtained by Foyo-Moreno model (black dots), modified CPCR2 model (red dots) and SBDART model (green dots) vs. cosine of solar zenith angle ($\cos\theta_z$), for background atmospheric aerosol condition. (For interpretation of the references to colour in this figure legend, the reader is referred to the web version of this article.)

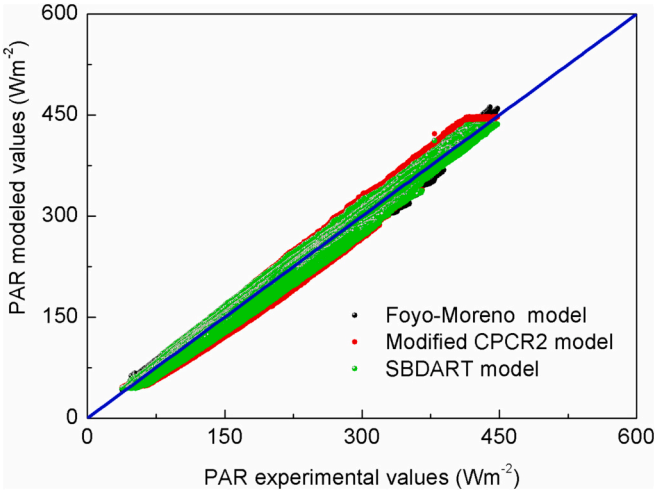

Fig. 7. Comparison of Photosynthetically active radiation (PAR) modelled values obtained by Foyo-Moreno model (black dots), modified CPCR2 model (red dots) and SBDART model (green dots) vs. PAR experimental values.

On the other hand, the model with higher values of PAR under clear-skies with background aerosol is the modified CPRC2 and the model with lower values for PAR under the same conditions is the SBDART (Fig. 6). In this work the SBDART model is considered as reference to compare with the other two methods, because the SBDART is a model commonly used in the determination of ARF (e.g. Sumit et al., 2012; Valenzuela et al., 2012). To compare the models we have used MBE (Mean bias error), RMSE (Root mean squared error), rRMSE (Relative root mean squared error), MABE (Mean absolute bias error), R^2 (Coefficient of determination), and MAPE (Mean absolute percentage error). Table 1 shows the definitions and Table 2 the results for the three years.

As we can observed from the Table 2, for all years and for the two models R^2 is above 0,99 indicating the good performance of the models. RMSE are between 25,0 and 32,0 Wm^{-2} for the modified CPCR2 method and 12,0 and 14,0 Wm^{-2} for the proposed max-k_t method, being the new method closer to SBDART model, but both overestimating in comparison to SBDART model. Respect to the values of rRMSE, except for the year

Table 1
Summary of statistical metrics used in the study.

Metrics	Equation
Determination coefficient, R^2	$1-\frac{\sum_{i=1}^{n}(x_i-y_i)^2}{\sum_{i=1}^{n}(x_i-\bar{x})^2}$
Mean bias error, MBE	$\frac{1}{n}\sum_{i=1}^{n}(y_i-x_i)$
Root mean squared error, RMSE	$\sqrt{\frac{1}{n}\sum_{i=1}^{n}(y_i-x_i)^2}$
Relative root mean squared error, rRMSE	$\frac{\sqrt{\frac{1}{n}\sum_{i=1}^{n}(y_i-x_i)^2}}{\bar{x}}\times 100$
Mean percentage error, MPE	$\frac{1}{n}\sum_{i=1}^{n}\frac{y_i-x_i}{x_i}\times 100$
Relative standard desviation, RSD	$\sqrt{\frac{1}{n}\sum_{i=1}^{n}\left(\frac{y_i-x_i}{x_i}\right)^2}\times 100$
Mean absolute bias error, MABE	$\frac{1}{n}\sum_{i=1}^{n}\lvert y_i-x_i\rvert$
Mean abstolute percentage error, MAPE	$\frac{1}{n}\sum_{i=1}^{n}\left\lvert\frac{y_i-x_i}{x_i}\right\rvert\times 100$
	x_i experimental values
	y_i estimated values
	$\bar{x}$ mean of experimental values
	n number of values

Table 2
Statistical results for comparison between SBDART model (considered as reference) and models Foyo-Moreno and CPCR2.

		Foyo-Moreno			CPCR2	
	2017	2018	2020	2017	2018	2020
R^2	0.998	0.999.	0.998	0.999	0.999	0.999
MBE	11 Wm^{-2}	13 Wm^{-2}	13 Wm^{-2}	25 Wm^{-2}	31 Wm^{-2}	26 Wm^{-2}
RMSE	12 Wm^{-2}	14 Wm^{-2}	14 Wm^{-2}	25 Wm^{-2}	32 Wm^{-2}	26 Wm^{-2}
RMSEr	4.7%	5.2%	4.9%	9.8%	11.6%	9.2%
MPE	5.3%	5.8%	5.4%	12.5%	4.2%	11,3%
RSD	6.4%	6.9%	6.3%	14.8%	16.4%	13.2%
MABE	11 Wm^{-2}	13 Wm^{-2}	13 Wm^{-2}	25 Wm^{-2}	31 Wm^{-2}	26 Wm^{-2}
MAPE	5.3%	5.8%	5.4%	12.5%	14.2%	11.3%

2018 the values are always lower than 10% for both models and in fact, for the max-k_t method is lower than 5,2%, thus the success of the model comparison is very good. Also, considering the values of MAPE, the new method for all years is lower than 5,8% and for CPCR2 model lower than 14,2%, thus this proposal is of high prediction accuracy and the other model is of good prediction.

It is interesting to point out the validity of one empirical model used in this work in comparison to physical models. In general, the empirical models have advantages of simple formulation and ease of use. They can also produce relatively accurate PAR estimations in a local area, but the disadvantage of these models is that they are usually restricted by local meteorological conditions due to their dependency on local observational data. The model used here for PAR with aerosols (Foyo-Moreno et al., 2017) has been evaluated by Ferrera-Cobos et al. (2021) in various sites of Spain with very different climatic characteristics showing good results. Besides, that model was also evaluated for sites located in Argentina and Japan with very low errors (Foyo-Moreno et al., 2017). These results for the PAR estimation under clear skies with and without aerosols are very close to physical models such as SBDART, and allows to confirm the validity of this proposed technique, with the added advantage that only needs to estimate ARF the solar position through the cosine of θ_z and k_t, i.e., the proposed max-k_t method only requires measurements of global irradiance, in contrast to the theoretical models where many input variables are required.

6. Conclusions

This work presents a new method, max-k_t method, to estimate aerosol radiative forcing (ARF) for photosynthetically active radiation (PAR). The main basis of the max-k_t method is the dependence of clearness index (k_t) on solar position for clear skies, being an important and not trivial issue the selection of clear skies, considering the different criteria existing in the scientific community. On the other hand, the fit of this relationship will be different depending on the site but this method might be applied with measurements of global irradiance for a given site to calculate this index. An automated algorithm to identify clear periods would facilitate the task, however, the drawback is that some of the more exact methods use diffuse irradiance, not always available.

The new method has been compared with the simulation obtained from widely used physical models (SBDART and modified CPRC2), using one full year of data (2020) retrieved in a location in the Southwest Mediterranean, and two years more have been used to extend the results. The values obtained are very different, with a mean value of ARF of (-14 ± 4) Wm^{-2} for the SBDART model, (-35 ± 2) Wm^{-2} for the CPRC2 model and (-23 ± 11) Wm^{-2} for the max-k_t method for the year 2020. The main differences come from the estimation of PAR without aerosols and in this comparison the SBDART model has been considered as reference, being the model of Foyo-Moreno et al. (2017) (basis of the max-k_t method) which present results very close to SBDART model. This result confirms the validity of this proposal, with the advantage of easily obtaining ARF from irradiance global measurements available in many radiometric stations, since it only needs two variables as input data, solar position and clearness index (k_t), in contrast to physical models which require more input variables.

Values obtained for ARF using the max-k_t method presented a clear seasonal pattern with maximum in summer ($(-30{,}7 \pm 9{,}0)$ Wm^{-2} in August during 2017, $(-40{,}1 \pm 11{,}8)$ Wm^{-2} in June during 2018 and $(-28{,}8 \pm 7{,}7)$ Wm^{-2} in July during 2020) and minimum values in winter ($(-8{,}1 \pm 5{,}1)$ Wm^{-2} in January during 2017, $(-5{,}7 \pm 5{,}8)$ Wm^{-2} in December during 2018 and $(-7{,}8 \pm 5{,}4)$ Wm^{-2} in December) during 2020. Also, a dependence on solar position has been detected for the years 2017 and 2020, increasing ARF values with solar zenith angle (θ_z) up to the range 45-60° and then decreasing to values close to zero for Sun near the horizon.

This proposed technique presents the main advantage that does not require the previous knowledge of all inputs requested by physical models and it is very useful for the operational estimation of ARF when computational load and great accuracy in PAR are major issues. However, the applicability of this method should be tested at another sites in order to fully manifest its universality.

Declaration of Competing Interest

The authors declare that they have no known competing financial interests or personal relationships that could have appeared to influence the work reported in this paper. (For interpretation of the references to colour in this figure legend, the reader is referred to the web version of this article.)

Data availability

Data will be made available on request.

Acknowledgements

This work was supported by the Spanish Ministry of Economy and Competitiveness through projects CGL2017-90884-REDT, PID2020-120015RB-I00, PID2020-117825GB-C21, PID2020-117825GB-C22 and PID2021-128008OB-I00, by the Andalusia Regional Government, University of Granada and FEDER funds through project B-RNM-524-UGR20, A-RNM-430-UGR20, P20-00136 and P18-RT-3820. This

research was partially supported by the Scientific Units of Excellence Program (grant no. UCE-PP2017-02). The authors thankfully acknowledge the FEDER program for the instrumentation used in this work. Funding for open access charge: University of Granada / CBUA.

References

Alados, I., Alados Arboledas, L., 1999. Validation of an empirical model for photosynthetically active radiation. Int. J. Climatol. 19, 1145–1152. https://doi.org/10.1002/(SICI)1097-0088(199908)19:10<1145:AID-JOC428>3.0.CO;2-3.

Alados, I., Foyo-Moreno, I., Alados-Arboledas, L., 1996. Photosynthetically active radiation: measurements and modelling. Agric. For. Meteor. 78, 121–131. https://doi.org/10.1016/0168-1923(95)02245-7.

Alados, I., Olmo, F.J., Foyo-Moreno, I., Alados-Arboledas, L., 2000. Estimation of photosynthetically active radiation under cloudy conditions. \ 102 (1), 39–50. https://doi.org/10.1016/S0168-1923(00)00091-5.

Alados, I., Foyo-Moreno, I., Olmo, F.J., Alados-Arboledas, L., 2002. Improved estimation of diffuse photosynthetically active radiation using two spectral models. \ 111 (1), 1–12. https://doi.org/10.1016/S0168-1923(02)00010-2.

Alados-Arboledas, L., Olmo, F.J., Alados, I., Pérez, M., 2000. Parametric models to estimate photosynthetically active radiation in Spain. \ 101, 187–201. https://doi.org/10.1016/S0168-1923(99)00163-X.

Alados-Arboledas, L., Müller, D., Guerrero-Rascado, J.L., Navas-Guzman, F., Pérez-Ramírez, D., Olmo, F.J., 2011. Optical and microphysical properties of fresh biomass burning aerosol retrieved by Raman lidar, and star-and sun-photometry. J. Geophys. Res. Lett. 38 https://doi.org/10.1029/2010GL045999.

Albrecht, B.A., 1989. Cloud microphysics, and fractional cloudiness. Science 45 (4923), 1227–1230. https://doi.org/10.1126/science.245.4923.1227.

Antón, M., Gil, J.E., Fernández-Gálvez, J., Lyamani, H., Valenzuela, A., Foyo-Moreno, I., Olmo, F.J., Alados-Arboledas, L., 2011. Evaluation of the aerosol forcing efficiency in the UV erythemal range at Granada, Spain. J. Geophys. Res. 116 (D20), D20214. https://doi.org/10.1029/2011JD016112.

Baars, H., Ansmann, A., Ohneiser, K., Haarig, M., Engelmann, R., Althausen, D., Hanssen, I., Gausa, M., Pietruczuk, A., Szkop, A., Stachlewska, I.S., Wang, D., Reichardt, J., Skupin, A., Mattis, I., Trickl, T., Vogelmann, H., Navas-Guzman, F., Haefele, A., Pappalardo, G., 2019. The unprecedented 2017–2018 stratospheric smoke event: decay phase and aerosol properties observed with the EARLINET. Atmos. Chem. Phys. 19 (23), 15183–15198. https://doi.org/10.5194/acp-19-15183-2009.

Bergamo, A., Tafuro, A.M., Kinne, S., De Tomasi, F., Perrone, R.C., 2008. Monthly-averaged anthropogenic aerosol direct radiative forcing over the Mediterranean based on AERONET aerosol properties. Atmos. Chem. Phys. 8, 6995–7014. https://doi.org/10.5194/acp-8-6995-2008.

Bird, R.E., Riordan, C., 1986. Simple solar spectral model for direct and diffuse irradiance on horizontal and tilted planes at the Earth's surface for cloudless atmospheres. J. Clim. Appl. Meteorol. 25 (1), 87–97.

Cachorro, V.E., Toledano, C., Prats, N., Sorribas, M., Mogo, S., Berjon, A., Torres, B., Rodrigo, R., de la Rosa, J., Frutos, De, 2008. The strongest desert dust intrusion mixed with smoke over the Iberian Peninsula registered with Sun photometry. J. Geophys. Res. 113 https://doi.org/10.1029/2007JD009582. D14S04.

Cariñanos, P., Foyo-Moreno, I., Alados, I., Guerrero-Rascado, Juan Luis, Ruiz Peñuela, S., Titos, G., Cazorla, A., Alados-Arboledas, L., Díaz De La Guardia, C., 2021. Bioaerosols in urban environments: trends and interactions with pollutants and meteorological variables based on quasi-climatological series. J. Environ. Manag. 282, 111963 https://doi.org/10.1016/j.jenvman.2021.111963.

Cariñanos, P., Guerrero-Rascado, J.L., Valle, A.M., Cazorla, A., Titos, G., 2022. Assessing pollen extreme events over a Mediterranean site: role of local surface meteorology. Atmos. Environ. 272, 118928.

Charlson, R.J., Langner, J., Rodhe, H., Leovy, C.B., Warren, S.G., 1991. Perturbation of the northern hemisphere radiative balance by backscattering from anthropogenic sulfate aerosols. Tellus A: Dyn. Meteorol. Oceanogr. 43 (4), 152–163.

Di Biagio, C., di Sarra, A., Meloni, D., Monteleone, F., Piacentino, S., Sferlazzo, D., 2009. 633 Measurements of Mediterranean aerosol radiative forcing and influence of the single 634 scattering albedo. J. Geophys. Res. 114 (D6), D06211. https://doi.org/10.1029/2008JD011037.

Di Biagio, C., di Sarra, A., Meloni, D., 2010. Large atmospheric shortwave radiative forcing by Mediterranean aerosols derived from simultaneous ground-based and spaceborne observations and dependence on the aerosol type and single scattering albedo. J. Geophys. Res. 115 (D10), D10209. https://doi.org/10.1029/2009JD012697.

Esteve, A.R., Estellés, V., Utrillas, M.P., Martínez-Lozano, J.A., 2014. Analysis of the aerosol radiative forcing over a Mediterranean urban coastal site. Atmos. Res. 137, 195–204.

Fernández, A.J., Sicard, M., Costa, M.J., Guerrero-Rascado, J.L., Gómez-Amo, J.L., Molero, F., Barragán, R., Basart, S., Bortoli, D., Bedoya-Velásquez, A.E., Utrillas, M. P., Salvador, P., Granados-Muñoz, M.J., Potes, M., Ortiz-Amezcua, P., Martínez-Lozano, J.A., Artíñano, B., Muñoz-Porcar, C., Salgado, R., Román, R., Pujadas, M., 2019. Extreme, wintertime Saharan dust intrusion in the Iberian Peninsula: lidar monitoring and evaluation of dust forecast models during the February 2017 event. Atmos. Res. 228, 223–241.

Ferrera-Cobos, F., Vindel, J.M., Wane, O., Navarro, A.A., Zarzalejo, L.F., Valenzuela, R. X., 2021. Combination of models to generate the first PAR Maps for Spain. Remote Sens. 13, 4950. https://doi.org/10.3390/rs13234950.

Foyo-Moreno, I., Alados, I., Antón, M., Fernández-Gálvez, J., Cazorla, A., Alados-Arboledas, L., 2014. Estimating aerosol characteristics from solar irradiance measurements at an urban location in southeastern Spain: aerosol properties from solar irradiance. J. Geophys. Res.-Atmos. 119 (4), 1845–1859. https://doi.org/10.1002/2013JD020599.

Foyo-Moreno, I., Alados, I., Alados-Arboledas, L., 2017. A new conventional regression model to estimate hourly photosynthetic photon flux density under all sky conditions. Int. J. Climatol. 37, 1067–1075. https://doi.org/10.1002/joc.5063.

Foyo-Moreno, I., Alados, I., Guerrero-Rascado, J.L., Lyamani, H., Pérez-Ramírez, D., Olmo, F.J., Alados-Arboledas, L., 2019. Contribution to column-integrated aerosol typing based on Sun-photometry using different criteria. Atmos. Res. 224, 1–17. https://doi.org/10.1016/j.atmosres.2019.03.007.

Garcia-Herrera, R.F., Lionello, P., Ulbrich, U., 2014. Preface: understanding dynamics and current developments of climate extremes in the Mediterranean Region. Nat. Hazards Earth Syst. Sci. 8.

Giles, D.M., Sinyuk, A., Sorokin, M.G., Schafer, J.S., Smirnov, A., Slutsker, I., Eck, T.F., Holben, B.N., Lewis, J.R., Campbell, J.R., Welton, E.J., Korkin, S.V., Lyapustin, A.I., 2019. Advancements in the Aerosol Robotic Network (AERONET) Version 3 database – automated near-real-time quality control algorithm with improved cloud screening for Sun photometer aerosol optical depth (AOD) measurements. Atmos. Meas. Tech. 12 (1), 169–209. https://doi.org/10.5194/amt-12-169-2019.

Gkikas, A., Hatzianastassiou, N., Mihalopoulos, N., Katsoulis, V., Kazadzis, S., Pey, J., Querol, X., Torres, O., 2013. The regime of intense desert dust episodes in the Mediterranean based on contemporary satellite observations and ground measurements. Atmos. Chem. Phys. 13 (23), 12135–12154. https://doi.org/10.5194/acp-13-12135-2013.

Gkikas, A., Obiso, V., Pérez García-Pando, C., Jorba, O., Hatzianastassiou, N., Vendrell, L., Basart, S., Solomos, S., Gasso, S., Baldasano, J.M., 2018. Direct radiative effects during intense Mediterranean desert dust outbreaks. Atmos. Chem. Phys. 18 (12), 8757–8787. https://doi.org/10.5194/acp-18-8757-2018.

Guerrero-Rascado, J.L., Ruiz, B., Alados-Arboledas, L., 2008. Multi-spectral Lidar characterization of the vertical structure of Saharan dust aerosol over southern Spain. Atmos. Environ. 42 (11), 2668–2681. https://doi.org/10.1016/j.atmosenv.2007.12.062.

Guerrero-Rascado, J.L., Olmo, F.J., Aviles-Rodríguez, I., Navas-Guzman, F., Pérez-Ramírez, D., Lyamani, H., Alados Arboledas, L., 2009. Extreme Saharan dust event over the southern Iberian Peninsula in september 2007: active and passive remote sensing from surface and satellite. Atmos. Chem. Phys. 9 (21), 8453–8469. https://doi.org/10.5194/acp-9-8453-2009.

Gueymard, C., 1989. A Two-band model for the calculation of clear sky solar irradiance, illuminance, and photosynthetically active radiation at the earth's surface. Sol. Energy 43, 253–265.

Halthore, R.S., Crisp, D., Schwartz, S.E., Anderson, G.P., Berk, A., Bonnel, B., Boucher, O., Chang, F.-L., Chou, M.-D., Clothiaux, E.E., Dubuisson, P., Fomin, B., Fouquart, Y., Freidenreich, S., Gautier, C., Kato, S., Laszlo, I., Li, Z., Mather, J.H., Plana-Fattori, A., Ramaswamy, V., Ricchiazzi, R., Shiren, Y., Trishchenko, A., Wiscombe, W., 2005. Intercomparison of shortwave radiative transfer codes andmeasurements. J. Geophys. Res. 110, D11206. https://doi.org/10.1029/2004JD005293.

Holben, B.N., Eck, T.F., Slutsker, I., Tanr'e, D., Buis, J.P., Setzer, A., Vermote, E., Reagan, J.A., Kaufman, Y.J., Nakajima, T., Lavenu, F., Jankowiak, I., Smirnov, A., 1998. AERONET—A federated instrument network and data archive for aerosol characterization. Remote Sens. Environ. 66 (1), 1–16. https://doi.org/10.1016/S0034- 4257(98)00031-5.

Huang, G., Liu, Q., Wang, Y., He, Q., Chen, Y., Jin, L., Liu, T., He, Q., Gao, J., Zhao, K., Liu, P., 2020. The accuracy improvement of clear-sky surface shortwave radiation derived from CERES SSF dataset with a simulation analysis. Sci. Total Environ. 749, 141671 https://doi.org/10.1016/j.scitotenv.2020.141671.

Iqbal, M., 1983. An Introduction to Solar Radiation. Academic Press, Canada.

Jacovides, C.P., Tymvios, F.S., Assimakopoulos, V.D., Kaltsounides, N.A., 2007. The dependence of global and diffuse PAR radiation components on sky conditions at Athens, Greece. Agric. For. Meteorol. 143, 277–287.

Jonard, F., De Cannière, S., Brüggemann, N., Gentine, P., Short Gianotti, D.J., Lobet, G., Miralles, D.G., Montzka, C., Pagán, B.R., Rascher, U., Vereecken, H., 2020. Value of sun-induced chlorophyll fluorescence for quantifying hydrological states and fluxes: current status and challenges. Agric. For. Meteorol. 291, 108088 https://doi.org/10.1016/j.agrformet.2020.108088.

Justus, C.G., Paris, M.V., 1985. A model of solar spectral irradiance and radiative at the bottom and top of a cloudless atmosphere. J. Appl. Meteorol. Climatol. 24, 193–205. https://doi.org/10.1175/1520-0450(1985)024<0193:AMFSSI>2.0.CO;2.

Khan, A., Dierssen, H., Scambos, T.A., Höfer, J., Corde, R.R., 2012. Spectral characterization, radiative forcing and pigment content of coastal Antarctic snow algae: approaches to spectrally discriminate red and green communities and their impact on snowmelt. Cryosphere 15, 133–148. https://doi.org/10.5194/tc-15-133-2021.

Kondratyev, K.Y., 1969. Radiation in the Atmosphere. Academic.Press, New York.

Kundu, S., Borgohain, A., Barman, N., Devi, M., Raju, P., 2018. Spatial variability and radiative impact of aerosol along the Brahmaputra River Valley in India: results from a campaign. J. Environ. Prot. 9, 405–430. https://doi.org/10.4236/jep.2018.94026.

Landsberg, J.J., Waring, R.H., 1997. A generalised model of forest productivity using simplified concepts of radiation-use efficiency, carbon balance and partitioning. For. Ecol. Manag. 95 (3), 209–228.

Lanetz, A., Lyubansky, V., Setter, I., Evseev, E., Kudish, A., 2005. Inter-comparison of different methods for estimating clear-sky global radiation for the Negev region of Israel. In: Proceeding of the 2nd SOLARIS Conference, Athens, Greece.

Lee, J., Kim, J., Song, C.H., Kim, S.B., Chun, Y., Sohn, B.J., Holben, B.H., 2010. Characteristics of aerosol types from AERONET sunphotometer measurements. Atmos. Environ. 44, 3110–3117.

Lefèvre, M., Oumbe, A., Blanc, P., Espinar, B., Gschwind, P., Qu, Z., Wald, L., Schroedter-Homscheidt, M., Hoyer-Klick, C., Arola, A., Benedetti, A., Kaiser, J.W., Morcrette, J. J., 2013. Atmos. Meas. Tech. 6, 2403–2418. https://doi.org/10.5194/amt-6-2403-2013.

Li, Z.Q., Lee, K.H., Wang, Y.S., Xin, J.Y., Hao, W.M., 2010. First observation-based estimates of cloud-free aerosol radiative forcing across China. J. Geophys. Res. 115 https://doi.org/10.1029/2009jd013306.

Liang, S., Wang, D., He, T., Yu, Y., 2019. Remote sensing of earth's energy budget: synthesis and review. Int. J. Digital Earth 12 (7), 737–780. https://doi.org/10.1080/17538947.2019.1597189.

Lohmann, U., Feichter, J., 2005. Global indirect aerosol effects: a review. Atmos. Chem. Phys. 5 (715–737), 2005. https://doi.org/10.5194/acp-5-715-2005.

Long, C.N., Ackerman, T.P., 2000. Identification of clear skies from broadband pyranometer measurements and calculation of downwelling shortwave cloud-effects. J. Geophys. Res. 105 (15), 609–626.

Lozano, I.L., Sánchez-Hernández, G., Guerrero-Rascado, J.L., Alados, I., Foyo-Moreno, I., 2021. Aerosol radiative effects in photosynthetically active radiation and total irradiance at a Mediterranean site from an 11-year database. Atmos. Res. 255, 105538 https://doi.org/10.1016/j.atmosres.2021.105538.

Luo, H., Han, Y., Lu, C.S., Yang, J., Wu, Y.H., 2019. Characteristics of surface solar radiation under different air pollution conditions over Nanjing, China: observation and simulation. Adv. Atmos. Sci. 36 (10), 1047–1059. https://doi.org/10.1007/s00376-019-9010-4.

Luthala, H., Tolvanen, K., Kalliola, R., 2013. Annual spatio-temporal variation of euphotic depth in the SW-Finnish archipelago, Baltic Sea. Oceanologia 55 (2), 359–373. https://doi.org/10.5697/oc.55-2.359.

Lyamani, H., Olmo, F.J., Alcántara, A., Alados-Arboledas, L., 2006a. Atmospheric aerosols during the 2003 heat wave in southeastern Spain I: spectral optical depth. Atmos. Environ. 40 (33), 6453–6464. https://doi.org/10.1016/j.atmosenv.2006.04.048.

Lyamani, H., Olmo, F.J., Alcantara, A., Alados-Arboledas, L., 2006b. Atmospheric aerosols during the 2003 heat wave in southeastern Spain II: microphysical columnar properties and radiative forcing. Atmos. Environ. 40 (33), 6465–6476. https://doi.org/10.1016/j.atmosenv.2006.04.047.

Lyamani, H., Olmo, F.J., Alados-Arboledas, L., 2010. Physical and optical properties of aerosols over an urban location in Spain: seasonal and diurnal variability. Atmos. Chem. Phys. 10, 239–254.

Ma, R., Letu, H., Yang, K., Wang, T., Shi, C., Xu, J., Chi, J., 2020. Estimation of surface shortwave radiation from Himawari −8 satellite data based on a combination of radiative transfer and deep neural network. IEEE Trans. Geosci. Remote Sens. 58, 5304–5316. https://doi.org/10.1109/TGRS.2019.2963262.

Mahowald, N., Lindsay, K., Rothenberg, D., Doney, S.C., Moore, J.K., Thornton, P., Randerson, J.T., Jones, C.D., 2011. Desert dust and anthropogenic aerosol interactions in the Community climate System Model coupled-carbon-climate model. Biogeosciences 8, 387–414. https://doi.org/10.5194/bg-8-387-2011.

Mateos, D., Antón, M., Toledano, C., Cachorro, V.E., Alados-Arboledas, L., Sorribas, M., Costa, M.J., Baldasano, J.M., 2014. Aerosol radiative effects in the ultraviolet, visible, and near-infrared spectral ranges using long-term aerosol data series over the Iberian Peninsula. Atmos. Chem. Phys. 14 (24), 13497–13514. https://doi.org/10.5194/acp-14-13497-2014.

Meloni, D., di Sarra, A., Di Iorio, T., Fiocco, G., 2005. Influence of the vertical profile of Saharan dust on the visible direct radiative forcing. J. Quant. Spectrosc. Radiat. Transf. 93 (4), 397–413. https://doi.org/10.1016/j.jqsrt.2004.08.035.

Mercado, L.M., Bellouin, N., Sitch, S., Boucher, O., Huntingford, C., Wild, M., Cox, P.M., 2009. Impact of changes in diffuse radiation on the global land carbon sink. Nature 458, 1014–1017. https://doi.org/10.1038/nature07949.

Navas-Guzman, F., Müller, D., Bravo-Aranda, J.A., Guerrero-Rascado, J.L., Granados-Muñoz, M.J., Pérez-Ramírez, D., Olmo, F.J., Alados-Arboledas, L., 2013. Eruption of the Eyjafjallajokull Volcano in spring 2010: Multiwavelength Raman lidar measurements of sulphate particles in the lower troposphere. J. Geophys. Res.-Atmos. 118 (4), 1804–1813. https://doi.org/10.1002/jgrd.50116.

Olmo, F.J., Foyo-Moreno, I., Tovar, J., Alados-Arboledas, I., 2001. Performance reduction of solar irradiance parametric models due to limitations in required aerosol data: case of the CPCR2 model. Theor. Appl. Climatol. 69, 253–263.

Ortiz-Amezcua, P., Guerrero-Rascado, J.L., Granados-Muñoz, M.J., Bravo-Aranda, J.A., Alados-Arboledas, L., 2014. Characterization of atmospheric aerosols for a long range transport of biomass burning particles from Canadian forest fires over the southern Iberian peninsula in July 2013. Optica Pura y Aplicada 47 (1), 43–49.

Ortiz-Amezcua, P., Guerrero-Rascado, J.L., Granados-Muñoz, M.J., Benavent-Oltra, J.A., Bockmann, C., Samaras, S., Stachlewska, I.S., Janicka, Ł., Baars, H., Bohlmann, S., Alados-Arboledas, L., 2017. Microphysical characterization of long-range transported biomass burning particles from North America at three EARLINET stations. Atmos. Chem. Phys. 17 (9), 5931–5946. https://doi.org/10.5194/acp-17-5931-2017.

Pei, F., Li, X., Liu, X., Lao, C., 2013. Assessing the impacts of droughts on net primary productivity in China. J. Environ. Manag. 114, 362–371.

Perez, R., Ineichen, P., Seals, R., 1990. Modelling daylight-availability and irradiance components from direct and global irradiance. Sol. Energy 44 (5), 271–289.

Pérez-Ramírez, D., Lyamani, H., Smirnov, A., O'Neill, N.T., Veselovskii, I., Whiteman, D. N., Olmo, F.J., Alados-Arboledas, L., 2016. Statistical study of day and night hourly patterns of columnar aerosol properties using sun and star photometry. Rem. Sens. Clouds Atmos. XXI, 10001. https://doi.org/10.1117/12.2242372, 100010K.

Potter, C., Boriah, S., Steinbach, M., Kumar, V., Klooster, S., 2007. Terrestrial vegetation dynamics and global climate controls. Clim. Dyn. 31 (1), 67–78.

Potter, C., Boriah, S., Steinbach, M., Kumar, V., Klooster, S., 2008. Terrestrial vegetation dynamics and global climate controls in North America: 2001–05. Earth Interact. 12 (8), 1–12.

Prasad, A.K., Singh, S., Chauhan, S.S., Srivastava, M.K., Singh, R.P., Singh, R., 2007. Aerosol radiative forcing over the Indo-Gangetic plains during major dust storms. Atmos. Environ. 41 (29), 6289–6301.

Ramírez-Aliaga, P., Foyo-Moreno, I., Cariñanos, P., 2022. Effects of Environmental stress on the Pollen Viability of Ornamental Tree-Species in the City of Granada (South-Eastern Spain). Forests 13 (12), 2131.

Ramírez-Pérez, L.J., Morales-Díaz, A.B., de Alba-Romenus, K., González-Morales, S., Benavides-Mendoza, A., Juárez-Maldonado, A., 2017. Determination of micronutrient accumulation in greenhouse cucumber crop using a modeling approach. Agronomy 7, 79.

Ricchiazzi, P., Yang, S., Gautier, C., Sowle, D., 1998. SBDART: a research and teaching software tool for plane-parallel radiative transfer in the earth's atmosphere. Bull. Am. Meteorol. Soc. 79, 2101–2114. https://doi.org/10.1175/15200477.

Román, R., Antón, M., Valenzuela, A., Gil, G.L., Lyamani, H., De Miguel, A., 2013. Evaluation of the desert dust effects on global, direct and diffuse spectral ultraviolet irradiance. Tellus Ser. B Chem. Phys. Meteorol. 65 (1), 19578.

Salvador, P., Alonso-Perez, S., Pey, J., Artíñano, B., de Bustos, J.J., Alastuey, A., Querol, X., 2014. African dust outbreaks over the western Mediterranean Basin: 11-year characterization of atmospheric circulation patterns and dust source areas. Atmos. Chem. Phys. 14 (13), 6759–6775. https://doi.org/10.5194/acp-14-6759-2014.

Satheesh, S.K., Ramanathan, V., 2000. Large differences in tropical aerosol forcing at the top of the atmosphere and Earth's surface. Nature 405 (6782), 60–63. https://doi.org/10.1038/35011039.

Sicard, M., Guerrero-Rascado, J.L., Navas-Guzman, F., Preißler, J., Molero, F., Toḿs, S., Bravo-Aranda, J.A., Comeron, A., Rocadenbosch, F., Wagner, F., Pujadas, M., AladosArboledas, L., 2012. Monitoring of the Eyjafjallajokull volcanic aerosol plume over the Iberian Peninsula by means of four EARLINET lidar stations. Atmos. Chem. Phys. 12 (6), 3115–3130. https://doi.org/10.5194/acp-12-3115-2012.

Sicard, M., Granados-Muñoz, M.J., Alados-Arboledas, L., Barragán, R., Bedoya-Velásquez, A.E., Benavent-Oltra, J.A., Bortoli, D., Comerón, A., Córdoba-Jabonero, C., Costa, M.J., del Águila, A., Fernández, A.J., Guerrero-Rascado, J.L., Jorba, O., Molero, F., Muñoz-Porcar, C., Ortiz-Amezcua, P., Papagiannopoulos, N., Potes, M., Pujadas, M., Rocadenbosch, F., Rodríguez-Gómez, A., Román, R., Salgado, R., Salgueiro, V., Sola, Y., Yela, M., 2019. Ground/space, passive/active remote sensing observations coupled with particle dispersion modelling to understand the inter-continental transport of wildfire smoke plumes. Remote Sens. Environ. 232, 111294 https://doi.org/10.1016/j.rse.2019.111294.

Stocker, T.F., Qin, D., Plattner, G.K., Tignor, M., Allen, S.K., Boschung, J., Nauels, A., Xia, Y., Bex, V., Midgley, P.M., 2013. IPCC, 2013. Climate Change.

Sumit, K., Devara, P.C.S., Manoj, M.G., 2012. Multi-site characterization of tropical aerosols: Implications for regional radiative forcing. Atmos. Res. 106, 71–85.

Thevenard, D., Brunger, A., 2001. ASHRAE Research Project 1015-RP. Typical Weather Years for International Locations.

Titos, G., Foyo-Moreno, I., Lyamani, H., Querol, X., Alastuey, A., Alados-Arboledas, L., 2012. Optical properties and chemical composition of aerosol particles at an urban location: an estimation of the aerosol mass scattering and absorption efficiencies. J. Geophys. Res.-Atmos. 117 (D4).

Titos, G., Del Aguila, A., Cazorla, A., Lyamani, H., Casquero-Vera, J.A., Colombi, C., Cuccia, E., Gianelle, V., Močnik, G., Alastuey, A., Olmo, F.J., Alados-Arboledas, L., 2017. Spatial and temporal variability of carbonaceous aerosols: assessing the impact of biomass burning in the urban environment. Sci. Total Environ. 578, 613–625. https://doi.org/10.1016/j.scitotenv.2016.11.007.

Twomey, S., 1974. Pollution and the planetary albedo. Atmos. Environ. 8, 1251–1256.

Valenzuela, A., Olmo Reyes, F.J., Lyamani, H., Anton, M., Quirantes Sierra, A., Alados Arboledas, L., 2012. Aerosol radiative forcing during African desert dust events (2005–2010) over Southeastern Spain. Atmos. Chem. Phys. Discuss. 12, 6593–6622.

Wild, M., 2009. Global dimming and brightening: a review. J. Geophys. Res. 114, D00D16. https://doi.org/10.1029/2008JD011470, 2009.

Xia, X., Li, Z., Wang, P., Chen, H., Cribb, M., 2007a. Estimation of aerosol effects on surface irradiance based on measurements and radiative transfer model simulations in northern China. J. Geophys. Res. 112 https://doi.org/10.1029/2006JD008337.

Xia, X., Li, Z., Holben, B., Wang, P., Eck, T., Chen, H., Cribb, M., Zhao, Y., 2007b. Aerosol optical properties and radiative effects in the Yangtze Delta region of China. J. Geophys. Res. 112 https://doi.org/10.1029/2007JD008859.

Younes, S., Muneer, T., 2007. Clear-sky classification procedures and models using a world-wide data-base. Appl. Energy 84, 623–645.

Zempila, M.M., Taylor, M., Bais, A., Kazadzis, A., 2016. Modeling the relationship between photosynthetically active radiation and global horizontal irradiance using singular spectrum analysis. J. Quantitat. Spectrosc. Radiat.Transfer 182, 240–263.

Zhu, Z., Wang, L., Gong, W., Xiong, Y., Hu, B., 2015. Observation and estimation of photosynthetic photon flux density in Southern China. Theor. Appl. Climatol. 120 (3–4), 701–712. https://doi.org/10.1007/s00704-014-1204-1.